



LUND UNIVERSITY

Evolution of In-Cylinder Diesel Engine Soot and Emission Characteristics Investigated with Online Aerosol Mass Spectrometry

Malmborg, Vilhelm; Eriksson, Axel; Shen, Mengqin; Nilsson, Patrik; Gallo, Yann; Waldheim, Björn; Martinsson, Johan; Andersson, Övind; Pagels, Joakim

Published in:
Environmental Science and Technology

DOI:
[10.1021/acs.est.6b03391](https://doi.org/10.1021/acs.est.6b03391)

2017

Document Version:
Publisher's PDF, also known as Version of record

[Link to publication](#)

Citation for published version (APA):
Malmborg, V., Eriksson, A., Shen, M., Nilsson, P., Gallo, Y., Waldheim, B., Martinsson, J., Andersson, Ö., & Pagels, J. (2017). Evolution of In-Cylinder Diesel Engine Soot and Emission Characteristics Investigated with Online Aerosol Mass Spectrometry. *Environmental Science and Technology*, 51(3), 1876–1885.
<https://doi.org/10.1021/acs.est.6b03391>

Total number of authors:
9

General rights

Unless other specific re-use rights are stated the following general rights apply:
Copyright and moral rights for the publications made accessible in the public portal are retained by the authors and/or other copyright owners and it is a condition of accessing publications that users recognise and abide by the legal requirements associated with these rights.

- Users may download and print one copy of any publication from the public portal for the purpose of private study or research.
- You may not further distribute the material or use it for any profit-making activity or commercial gain
- You may freely distribute the URL identifying the publication in the public portal

Read more about Creative commons licenses: <https://creativecommons.org/licenses/>

Take down policy

If you believe that this document breaches copyright please contact us providing details, and we will remove access to the work immediately and investigate your claim.

LUND UNIVERSITY

PO Box 117
221 00 Lund
+46 46-222 00 00

Evolution of In-Cylinder Diesel Engine Soot and Emission Characteristics Investigated with Online Aerosol Mass Spectrometry

V. B. Malmborg,^{*,†} A. C. Eriksson,^{†,‡} M. Shen,[§] P. Nilsson,[†] Y. Gallo,[§] B. Waldheim,^{||} J. Martinsson,[‡] Ö. Andersson,[§] and J. Pagels[†]

[†]Division of Ergonomics and Aerosol Technology, Lund University, Box 118, SE-22100, Lund, Sweden

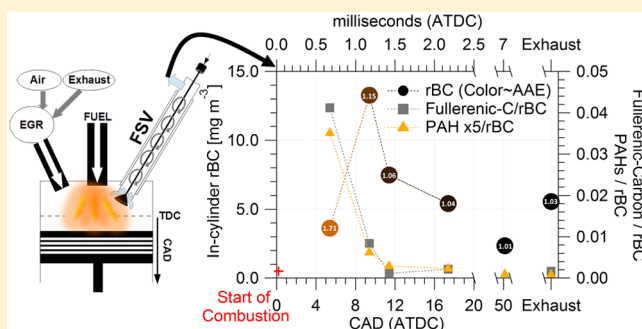
[‡]Division of Nuclear Physics, Lund University, Box 118, SE-22100, Lund, Sweden

[§]Division of Combustion Engines, Lund University, P.O. Box 118, SE-221 00, Lund, Sweden

^{||}Fluid and Combustion Simulations, Engine Development, Scania CV AB, SE-151 87, Södertälje, Sweden

S Supporting Information

ABSTRACT: To design diesel engines with low environmental impact, it is important to link health and climate-relevant soot (black carbon) emission characteristics to specific combustion conditions. The in-cylinder evolution of soot properties over the combustion cycle and as a function of exhaust gas recirculation (EGR) was investigated in a modern heavy-duty diesel engine. A novel combination of a fast gas-sampling valve and a soot particle aerosol mass spectrometer (SP-AMS) enabled online measurements of the in-cylinder soot chemistry. The results show that EGR reduced the soot formation rate. However, the late cycle soot oxidation rate (soot removal) was reduced even more, and the net effect was increased soot emissions. EGR resulted in an accumulation of polycyclic aromatic hydrocarbons (PAHs) during combustion, and led to increased PAH emissions. We show that mass spectral and optical signatures of the in-cylinder soot and associated low volatility organics change dramatically from the soot formation dominated phase to the soot oxidation dominated phase. These signatures include a class of fullerene carbon clusters that we hypothesize represent less graphitized, C₅-containing fullerenic (high tortuosity or curved) soot nanostructures arising from decreased combustion temperatures and increased premixing of air and fuel with EGR. Altered soot properties are of key importance when designing emission control strategies such as diesel particulate filters and when introducing novel biofuels.



INTRODUCTION

Diesel engines are a major source of air pollution as they emit large amounts of fine particulate matter and nitrogen oxides (NO_x) to the atmosphere. Diesel exhaust and soot particles can cause acute inflammatory responses in airways and peripheral blood,¹ decreased lung function,¹ asthmatic symptoms² and are classified as carcinogenic.³ Soot emissions (often referred to as black carbon; BC) also contribute to global warming through short-lived climate forcing.⁴ Consequently, reducing diesel engine NO_x and soot emissions is an essential measure to improve air quality and reduce the anthropogenic climate impact. For these reasons stringent diesel engine emission regulations of fine particulates and NO_x have been introduced in the European Union and the United States.

Modern diesel engines commonly apply exhaust gas recirculation (EGR) to reduce NO_x emissions. With EGR, a fraction of the engine inlet air is replaced by exhaust gases. This reduces the oxygen concentration and combustion temperature and consequently the rate at which NO_x forms.⁵ However, soot emissions increase rapidly with the decreasing inlet oxygen (O₂) concentration.^{6,7}

Soot emissions from diesel engines are determined by two competing in-cylinder processes: soot formation and soot oxidation.⁸ The soot formation rate is determined by the availability of acetylene, the formation of polycyclic aromatic hydrocarbons (PAHs) and the inception of soot particles,⁹ all of which are processes that depend strongly on temperature and local mixing of fuel and air. Soot oxidation (removal) depends strongly on the availability of hydroxyl radicals, O₂ and the temperature. The soot reactivity toward oxidation also depends strongly on the soot nanostructure^{10,11} and surface oxygen content.¹¹ Soot reactivity is of key importance when designing and optimizing diesel particulate filters (DPFs), the most important and efficient soot particle emission mitigation technique in modern diesel vehicles.

Studying in-cylinder soot properties can provide fundamental information on the relationship between combustion con-

Received: July 6, 2016

Revised: December 20, 2016

Accepted: January 4, 2017

Published: January 4, 2017

ditions and soot properties in order to increase our understanding of the processes governing soot emissions. These properties include particle size, chemical composition (e.g., elemental carbon and organic components, including PAHs), microstructure (e.g., primary particle size, aggregate sizes, and morphology) and nanostructure (e.g., fringe length, tortuosity, and separation distance). A recently emerging topic is the identification of high curvature (high tortuosity) soot nanostructures found in biodiesel emissions¹² and in laboratory studies of partially premixed flames.¹³ These properties may influence soot formation and oxidation rates, as well as soot reactivity and thus the design and efficiency of DPFs. Moreover, combining in-cylinder particle characterization and exhaust characterization can improve our knowledge of the relationship between combustion conditions and the eventual toxicity of emitted soot particles, which in a complex way depends on soot size, surface area and reactivity, surface coating material (e.g., PAHs), and metal content.¹⁴

There are a number of established techniques for studying in-cylinder particle concentrations and properties. Engines modified to allow optical access¹⁵ have enabled noninvasive highly time-resolved studies of in-cylinder gases (oxidants, PAHs, etc.) using laser-induced fluorescence,^{16,17} and studies of soot concentration using laser-induced incandescence^{18,19} and laser extinction.²⁰ Recently, TEM grids were mounted inside a cylinder allowing detailed studies of particle nanostructure using high resolution transmission electron microscopy²¹ (HR-TEM). A total cylinder sampling system²² can be used for rapid (1 ms) extraction of the full cylinder volume from a single combustion cycle and to study soot properties using an array of off-line techniques including HR-TEM and Raman microscopy.^{23,24} Off-line techniques involve particle sampling, handling and often chemical processing that could lead to unintended changes in particle properties. Online aerosol measurement techniques are commonly used in ambient measurements to characterize particle properties directly in the aerosol phase, for example to investigate the transformation of climate-relevant soot properties upon aging in the atmosphere.²⁵ The direct radiative forcing of BC can be described by knowledge of soot morphology and coating thickness,²⁶ for which online characterization is essential.

Fast sampling valves^{27–29} (FSVs) are in-cylinder gas extraction techniques that enable particle characterization using online aerosol instruments. FSVs repeatedly extract a small volume of in-cylinder gases at a well-defined position in the combustion process. The repeated extraction produces a semicontinuous flow of in-cylinder gases, and because of the small volume sampled in each extraction, the FSV has a negligible impact on combustion.²⁹ Additionally, the aerosol extracted is averaged over a large number of fired cycles which decreases the sensitivity to cycle-to-cycle variations compared to other in-cylinder particle extraction techniques.

The soot particle aerosol mass spectrometer (SP-AMS) was recently developed³⁰ to enable online chemical analysis of soot particles. It enables chemical analysis of the soot core by overlapping a focused Nd:YAG laser beam ($\lambda = 1064$ nm) with a beam of particles, permitting decoupled vaporization and electron ionization (70 eV) and thus detection of highly refractory species such as elemental carbon and heteroatoms (e.g., oxygen in the solid carbon core) in a high resolution time-of-flight (HR-ToF) mass spectrometer. The SP-AMS also allows the composition of nonrefractory material (e.g., organic material coating the soot core) to be characterized by

vaporizing particles on a heated porous-tungsten vaporizer at 600 °C.³¹ Probing in-cylinder particles with the SP-AMS can therefore provide more detailed online information on the composition of the refractory soot core and of condensed nonrefractory material on soot particles than present laser diagnostic techniques, and without the potential artifacts associated with off-line particle analysis.

We combined an FSV²⁹ and the SP-AMS to directly and continuously probe the evolution of in-cylinder particle composition and concentration as combustion progressed in a modern heavy duty diesel engine. We specifically addressed the implementation of lowered combustion temperatures and increased premixing using EGR, and its effect on soot characteristics during combustion.

Our results show that in-cylinder soot processes exhibit two distinct phases: a soot formation dominated phase and a soot oxidation dominated phase. These soot phases are well described in the literature,^{24,32,33} which indicates that representative in-cylinder conditions were probed. We show that EGR decreases both soot oxidation and soot formation rates which results in increased soot and PAH emissions. Finally, at high EGR we identified fullerene-like carbon cluster signals in the SP-AMS mass spectra. These large carbon clusters are hypothesized to represent high tortuosity (curved) soot nanostructures, linking combustion with EGR to increased C₅ chemistry also found in selected premixed flames.¹³

■ MATERIALS AND METHODS

Engine Operation. A heavy-duty Scania D13 engine was operated at low load (5.5 bar IMEPg) and 1200 rpm. The common rail fuel injection pressure was set to 2000 bar, the air intake temperature and pressure were set to 337 K and 1.65 bar, respectively. The fuel used was Swedish diesel MK1 with ultralow sulfur content, a cetane number of 56.8, an aromatic content of 4.4 vol % and an alkane content of 95.6 vol %. A synthetic lubrication oil (Powerway GE 40, Statoil) was used. Engine conditions were altered by running the engine at no EGR (0%), 56% and 64% EGR. These three EGR levels corresponded to engine inlet air O₂ concentrations of 21%, 15%, and 13%, respectively. When introducing EGR, the start of fuel injection (SOI) was initiated earlier in order for CA50 (the crank angle position where 50% of the heat has been released) to remain approximately constant at 7.5 crank angle degrees after the top dead center (CAD ATDC). Regulated gas phase emissions were monitored for the three EGR concentrations, corresponding to 21%, 15%, and 13% inlet O₂, and were (in g/kWh): hydrocarbons (HC) 0.113, 0.054, 0.046; carbon monoxide (CO) 0.41, 0.57, 1.99; nitrogen oxides (NO_x) 11.2, 0.27, 0.08, respectively. For a complete description of the engine and the operating conditions, the reader is referred to Shen et al.²⁹

Aerosol Sampling and Dilution. To extract in-cylinder particles, a fast sampling valve²⁹ (FSV) was mounted on the cylinder head by replacing one of the exhaust ports, with the sampling position located between two adjacent fuel jets. The valve is actuated by a solenoid hammer and in-cylinder gases were repeatedly extracted at a precise timing in the combustion process. The reported sampling times represent the opening of the FSV and the sampling resolution of the FSV (i.e., the duration that the valve is open) was estimated to less than 0.5–1 ms or 4–6 CAD, see Supporting Information (SI). The NO_x concentrations increased rapidly during the combustion and reached a plateau concentration in the late combustion cycle

(SI Figure S1) consistent with the exhaust NO_x concentration (within 30%). The FSV working principles and an estimation of the sampling resolution and particle losses are presented in the SI. After exiting the FSV, the extracted aerosol was diluted in three stages with a nominal dilution factor of 700 times and transported to the instruments. The dilution system is elaborated in detail in the SI together with a schematic (SI Figure S2).

Aerosol Characterization. Particle chemical composition was investigated with a soot-particle aerosol mass spectrometer³⁰ (Aerodyne Inc. Billerica, MA). The SP-AMS was run in single or dual vaporizer mode. In the single vaporizer mode, particles are flash vaporized upon impaction on a heated (600 °C) tungsten surface. In the dual vaporizer mode, particles containing rBC are vaporized using an intracavity Nd:YAG laser (1064 nm). The vapors are then ionized (70 eV electron ionization) and detected in a HR-ToF mass spectrometer. The SP-AMS allows efficient sampling of particles in the diameter range $\sim 70\text{--}500\text{ nm}$ ^{34,35} (vacuum aerodynamic diameter). The SP-AMS setup and calibration is further detailed in the SI.

The equivalent BC mass concentration and absorption angstrom exponent (AAE) were analyzed using an aethalometer³⁶ (model AE33, Magee Scientific). A scanning mobility particle sizer (SMPS, classifier model 3071, CPC 3010, TSI Inc.) was used to measure the particle mobility size distribution. The in-cylinder diesel soot concentration was measured simultaneously using the SP-AMS and the aethalometer. The rBC mass concentration correlated well with the equivalent BC mass measured with the aethalometer ($r^2 = 0.99$) with an rBC to BC ratio of 0.18 (SI Figure S9). This difference between the two instruments was likely caused by lower SP-AMS collection efficiency³⁷ for diesel soot compared to the calibrant (Regal Black) and differences between optical detection (aethalometer) and chemical detection (SP-AMS). Reported rBC concentrations have been scaled to the BC concentrations by the factor 1/0.18.

To quantify the contribution of particle phase in-cylinder PAHs to the total organic aerosol (OA), molecular masses corresponding to nine parent peaks of common PAH isomers between MW 202 and MW 300 ($\text{C}_{16}\text{H}_{10}$ and $\text{C}_{24}\text{H}_{12}$) were included. Smaller PAHs (with 2–3 rings, MW < 202) were not included in the analysis due to their high vapor pressure and lack of AMS analysis of pure lab standards. We accounted for the relative abundance of the parent peaks in the mass spectra (~ 0.25) found in previous laboratory calibrations for 7 PAH isomers.³⁸

RESULTS AND DISCUSSION

In-Cylinder Soot Formation and Oxidation. The engine was operated at three levels of EGR corresponding to 21% (no EGR), 15% and 13% inlet O_2 concentrations. At each level of EGR, the FSV was used to extract in-cylinder gas and particles at a number of positions during the combustion cycle. The reported in-cylinder concentrations were converted to standard temperature and pressure and reported in mg m^{-3} . The positions in the combustion cycle were chosen so that the soot formation dominated phase (increasing rBC concentration), the soot peak and the soot oxidation dominated phase (decreasing rBC concentration) were distinguishable.

The apparent rate of heat release (aRoHR) derived from the in-cylinder pressure data is presented in Figure 1a. The start of injection (SOI) occurred earlier when EGR was applied and the start of combustion (SOC) was delayed, which increased the

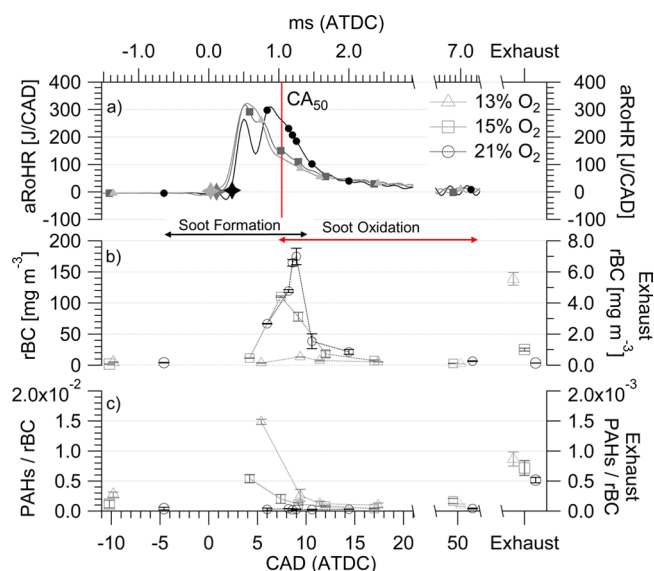


Figure 1. (a) In-cylinder heat release rates. Stars represent the start of combustion. The following symbols represent the aerosol sampling positions: triangles, 13% inlet O_2 ; squares, 15% inlet O_2 ; circles, 21% inlet O_2 . The CA50 was kept constant when changing EGR and is illustrated by the vertical red line. (b) SP-AMS rBC (soot) mass concentration. (c) The relative concentration of PAHs to rBC as a function of the combustion cycle. The position in the combustion cycle when particles were sampled is shown in milliseconds (ms, top) and crank angle degrees (CAD, bottom) after the top dead center (ATDC, located at $t = 0$). Three levels of EGR are shown corresponding to 21%, 15%, and 13% O_2 inlet O_2 concentrations. Exhaust emission values are shown on the right axis. Black and red arrows show the soot formation dominated phase and soot oxidation dominated phase, respectively. Error bars represent standard errors of the mean.

time allowed for premixing of air and fuel by approximately 0.8 CAD when the inlet O_2 concentration was changed from 21% to 13%. The aRoHR was characterized by two well-defined peaks at 21% inlet O_2 concentration. The two peaks indicate premixed or partially premixed combustion (first peak) and spray driven combustion (second peak) which transitioned into diffusion controlled combustion when the fuel injection stopped. As a result of lowered temperatures and slower kinetics when EGR was introduced, the two peaks were poorly defined at 15% inlet O_2 concentration and only one peak was observed at 13% inlet O_2 concentration.

Due to the high in-cylinder temperatures, the in-cylinder soot mass was principally determined by the concentration of refractory black carbon (rBC). The in-cylinder rBC concentrations measured with the SP-AMS are presented in Figure 1b. The rBC concentration increased rapidly after SOC (“soot formation phase”), it reached a maximum shortly after CA50 (“soot peak”), it then decreased rapidly (“soot oxidation phase”). The soot peak concentration decreased strongly with increasing EGR which shows that soot formation rates were reduced by lower inlet O_2 concentrations. Most of the soot formation and oxidation observed in Figure 1b occurred within approximately 2 ms (14 CAD).

Exhaust rBC concentrations increased with increasing EGR: $0.14 (\pm 0.01) \text{ mg m}^{-3}$ at 21% inlet O_2 concentration; $1.03 (\pm 0.09) \text{ mg m}^{-3}$ at 15% inlet O_2 concentration; $5.67 (\pm 0.40) \text{ mg m}^{-3}$ at 13% inlet O_2 concentration. This shows that soot oxidation rates were significantly reduced by EGR and that soot

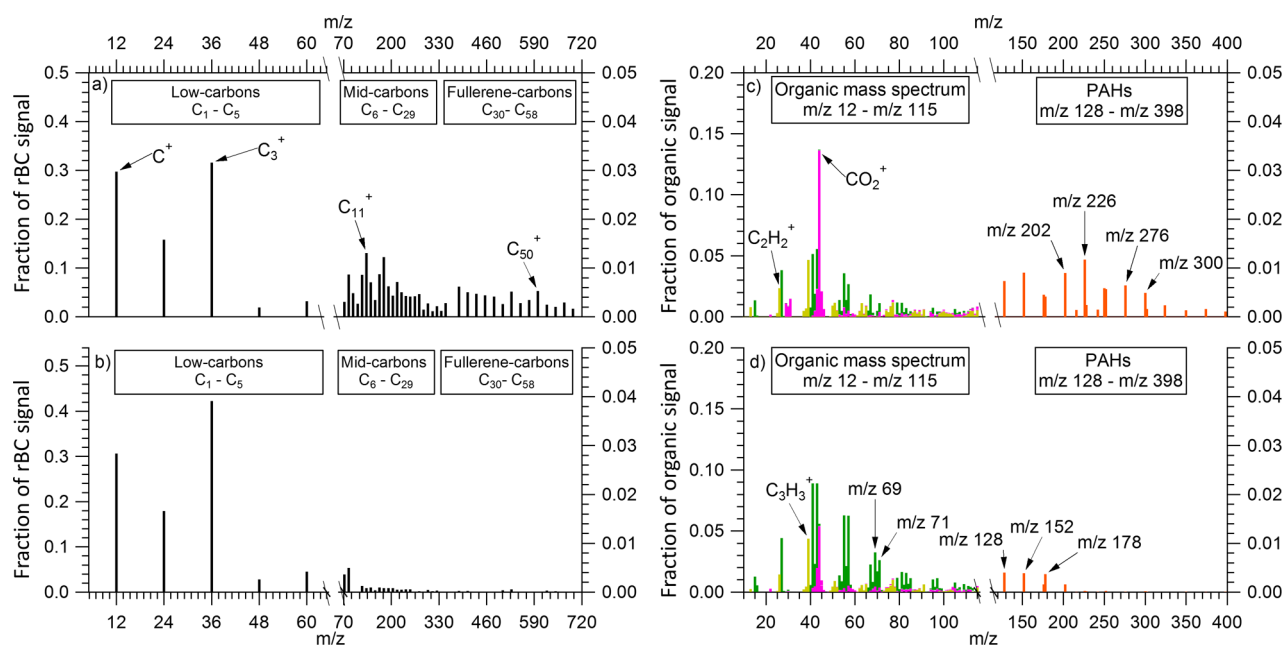


Figure 2. Refractory carbon cluster ion distributions and nonrefractory organic ion fragments at 13% inlet O_2 concentration during intense soot formation (a and c) at 5 CAD (ATDC) and after intense soot oxidation (b and d) at 18 CAD (ATDC). Refractory carbon clusters (a and b) are divided into low-carbon clusters ($C_1^+ - C_5^+$, left axis), midcarbon clusters ($C_6^+ - C_{29}^+$, right axis) and fullerene-carbon clusters with even carbon numbers ($C_{30}^+ - C_{58}^+$, right axis). Non-refractory organic ion fragments (c and d): aliphatic-like fragments ($C_xH_{y>x}^+$, green), aromatic-like fragments ($C_xH_{y<x}^+$, light green), oxidized organic fragments ($C_xH_yO_z^+$, magenta) are shown on the left axis, and PAHs (orange) are shown on the right axis.

oxidation was the dominant in-cylinder process that governed soot emissions in the raw engine exhaust. Lower soot oxidation rates with decreasing inlet O_2 concentrations have previously been shown to be the main cause of increased soot exhaust emissions with increasing EGR.^{33,39}

In-cylinder soot particle size distributions from the current measurements have been reported previously.²⁹ The exhaust soot size distributions for the three levels of EGR had the following geometrical mean mobility diameters and standard deviations: 54.8 ± 0.3 nm, 1.69 ± 0.01 at 21% inlet O_2 concentration; 46.9 ± 1.4 nm, 1.78 ± 0.02 at 15% inlet O_2 concentration; 70.3 ± 3.4 nm, 1.64 ± 0.01 at 13% inlet O_2 concentration.

Figure 1c shows the ratio of particle phase PAHs (4–6 ring PAHs, MW 202–300) relative to the rBC concentration. At 21% inlet O_2 concentration, the PAH to rBC ratio was low throughout the combustion cycle. At 13% and 15% inlet O_2 concentrations, elevated ratios were observed during the soot formation dominated phase that decreased as the combustion proceeded. These observations are consistent with large PAHs (in the size range from Pyrene, MW 202, to Coronene, MW 300) being involved in the formation and growth of soot particles. It also shows that lowered flame temperatures with EGR reduced the soot formation rates, and allowed the concentration of larger PAHs to accumulate. The particle phase PAH emissions in the exhaust (MW 202–300) increased with EGR and were $0.1 \mu\text{g m}^{-3}$ at 21% inlet O_2 concentration; $0.7 \mu\text{g m}^{-3}$ at 15% inlet O_2 concentration; and $4.8 \mu\text{g m}^{-3}$ at 13% inlet O_2 concentration. Thus, a fraction of the PAHs that accumulated during combustion with EGR survived, and the process led to increased emissions.

The soot trends presented in Figure 1b are generally consistent with in-cylinder soot trends obtained with highly time-resolved laser extinction measurements for similar EGR levels in a similar engine with optical access.^{33,40} Thus, the

combination of the FSV with online aerosol instruments is complementary to noninvasive optical techniques such as laser extinction.

Aerosol Mass Spectra of Soot in the Formation and Oxidation Dominated Phases. Figure 2 shows aerosol mass spectra of particles sampled from the soot formation dominated and oxidation dominated phases at 13% inlet O_2 (high EGR). The sizes of carbon clusters resulting from IR laser vaporization followed by electron ionization (70 eV) of the soot cores are shown in Figures 2a–b. The carbon clusters were grouped into low-carbons ($C_1^+ - C_5^+$), midcarbons ($C_6^+ - C_{29}^+$) and fullerene-carbons ($C_{30}^+ - C_{58}^+$). During both soot formation and oxidation, rBC was dominated by $C_1^+ - C_3^+$ ion fragments. Signals from larger mid- and fullerene-carbon clusters were pronounced in the soot formation phase (Figure 2a) and low in the oxidation phase (Figure 2b).

Low volatility organic species condense onto the soot particles and form the organic aerosol (OA) primarily when gases cool during extraction with the FSV and in the subsequent piping. The OA observed can be considered as the low volatility in-cylinder vapor species that will ultimately condense and form a soot coating in the engine exhaust. Aerosol mass spectra with the laser turned off (Figures 2c–d) were used to identify organic ion fragments (m/z 10–115) and the main PAH parent peaks (m/z 128–400). The organic mass spectra showed strong contributions from the hydrocarbon peaks $C_3H_5^+$ (m/z 41), $C_3H_7^+$ (m/z 43), $C_4H_7^+$ (m/z 55), and $C_4H_9^+$ (m/z 57). High signal intensity was also found at m/z 67, 69, 71 and m/z 81, 83, and 85. The origin of these hydrocarbon fragments are related to straight-chain alkanes (n -alkanes), branched alkanes ($C_nH_{2n+1}^+$) and cycloalkanes ($C_nH_{2n-1}^+$ and $C_nH_{2n-3}^+$) and they commonly dominate diesel exhaust OA.^{41–43} Ratios larger than 1 of the signal intensities at m/z 69 and 71, and at m/z 83 and 85 are likely only for an OA containing more than 95% lubrication oil.^{41,44} These ratios are

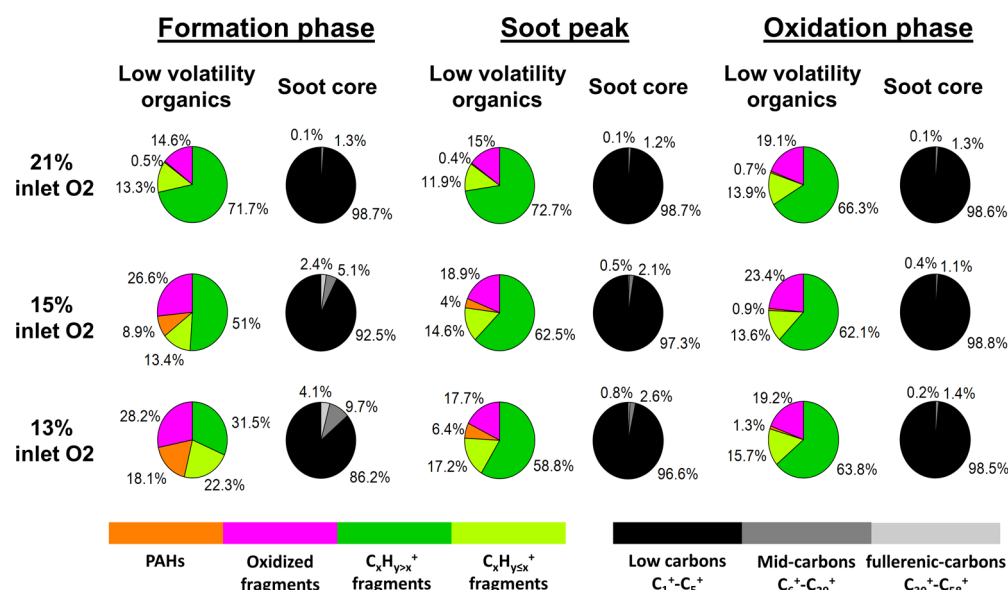


Figure 3. Soot chemical composition during the soot formation dominated phase, soot peak and soot oxidation dominated phase for 21%, 15% and 13% inlet O₂ concentrations. Left columns: grouped ion fragments originating from nonrefractory low volatility organics. Right columns: refractory carbon clusters from the soot core. Refractory soot core carbon clusters: low-carbons C₁⁺–C₅⁺ (black), midcarbons C₆⁺–C₂₉⁺ (dark gray) and fullerene-carbons C₃₀⁺–C₅₈⁺ (light gray). Nonrefractory low volatility organics: aliphatic-like fragments (C_xH_{y>x}⁺, green), aromatic-like fragments (C_xH_{y≤x}⁺, light green), oxidized organic fragments (C_xH_yO_z⁺, magenta) and PAHs (orange).

shown in SI Figure S10. OA was dominated by unburnt lubrication oil throughout the combustion cycle.

Aliphatic-like fragments originating mainly from saturated and unsaturated (or cyclic) compounds were grouped according to C_xH_{y>x}⁺. Other strong nonrefractory components included C₂H₂⁺, C₃H₃⁺, C₅H₃⁺ and C₆H₅⁺. These fragments and ions fulfilling the formula C_xH_{y≤x}⁺ originate mainly from aromatic or highly unsaturated aliphatic compounds and were assigned their own class in this study. Nonrefractory CO₂⁺ and other oxidized fragments were also assigned their own class (C_xH_yO_z⁺). The contribution of these two latter classes to OA decreased from the soot formation to the soot oxidation phase, with the mass spectra in the soot oxidation dominated phase being more similar to diesel exhaust OA signatures in the literature.⁴¹

Figures 2c–d show that PAHs were significantly more abundant in particles during soot formation. The larger PAHs decreased substantially in the soot oxidation phase, consistent with a large fraction of these PAHs having been converted to soot. Wang et al.³² found that the naphthalene concentration accounted for 26–84% of the total PAH mass throughout the combustion cycle. Thus, the signal detected with the AMS in the particle phase for the volatile PAHs (2–3 rings) may be only a fraction of their total concentrations. The reason we observed a signal from naphthalene, given its high vapor pressure, may be due to strong adsorption to the soot core surfaces and to a small extent fragmentation of larger PAHs during electron ionization.

Evolution of In-Cylinder Soot Characteristics. Figure 3 shows the evolution of soot properties between the soot formation and soot oxidation dominated phases at 21%, 15% and 13% inlet O₂ concentrations using the subgroups of rBC and OA described above. A clear transition of soot properties took place between the soot formation phase and soot oxidation phase at 15% and 13% inlet O₂ concentrations, but much smaller differences were observed at 21% O₂. In the refractory mass spectra of the soot cores, a transition in the

composition of rBC was observed at 15% and 13% inlet O₂ concentrations. The mass spectra had relatively high fractions of mid- and fullerene-carbons during the soot formation phase, and were completely dominated by low-carbons in the soot oxidation phase. During the soot formation phase, nonrefractory mass spectra of low volatility organics at 15% and 13% inlet O₂ concentrations were, in addition to aliphatic-like fragments (C_xH_{y>x}⁺), composed of substantial fractions of aromatic-like fragments (C_xH_{y≤x}⁺), oxidized organic fragments (C_xH_yO_z⁺), and PAHs.

Figure 4(a–f) shows a more detailed analysis of the in-cylinder soot evolution and comparison with the exhaust. Normalized rBC concentrations in Figure 4f are shown for reference to the evolution of in-cylinder soot mass. The fullerene-carbons (C_{30–58}⁺) shown in Figure 4a accounted for several percent of the rBC signals in the soot formation dominated phase at 15% and 13% inlet O₂ concentration. The fullerene-carbon fraction of rBC decreased gradually as the combustion proceeded. At 21% inlet O₂ concentration, fullerene-carbons represented a negligible fraction of rBC. As shown in SI, fullerene-carbon signals from the exhaust soot at 21% inlet O₂ concentration were only slightly higher than the nonrefractory organic background signal obtained with the laser turned off. At 13% inlet O₂ concentration, the signals from fullerene-carbon clusters in the exhaust were clearly higher than the organic background (SI Figure S12), although they were very low compared to the total signal from all refractory carbon clusters.

Recently, SP-AMS mass spectra of refractory carbon clusters from 12 different soot and manufactured carbon black sources were characterized.⁴⁵ Fullerene signals were not observed in mass spectra from graphitic (mature) soot, nor in amorphous carbon but they were detectable in biomass burning, ethylene flame soot and Nano-C fullerene black.⁴⁵ The authors concluded that fullerene signals in the SP-AMS may arise from carbon nanostructures that can form fullerenes upon heating.⁴⁵

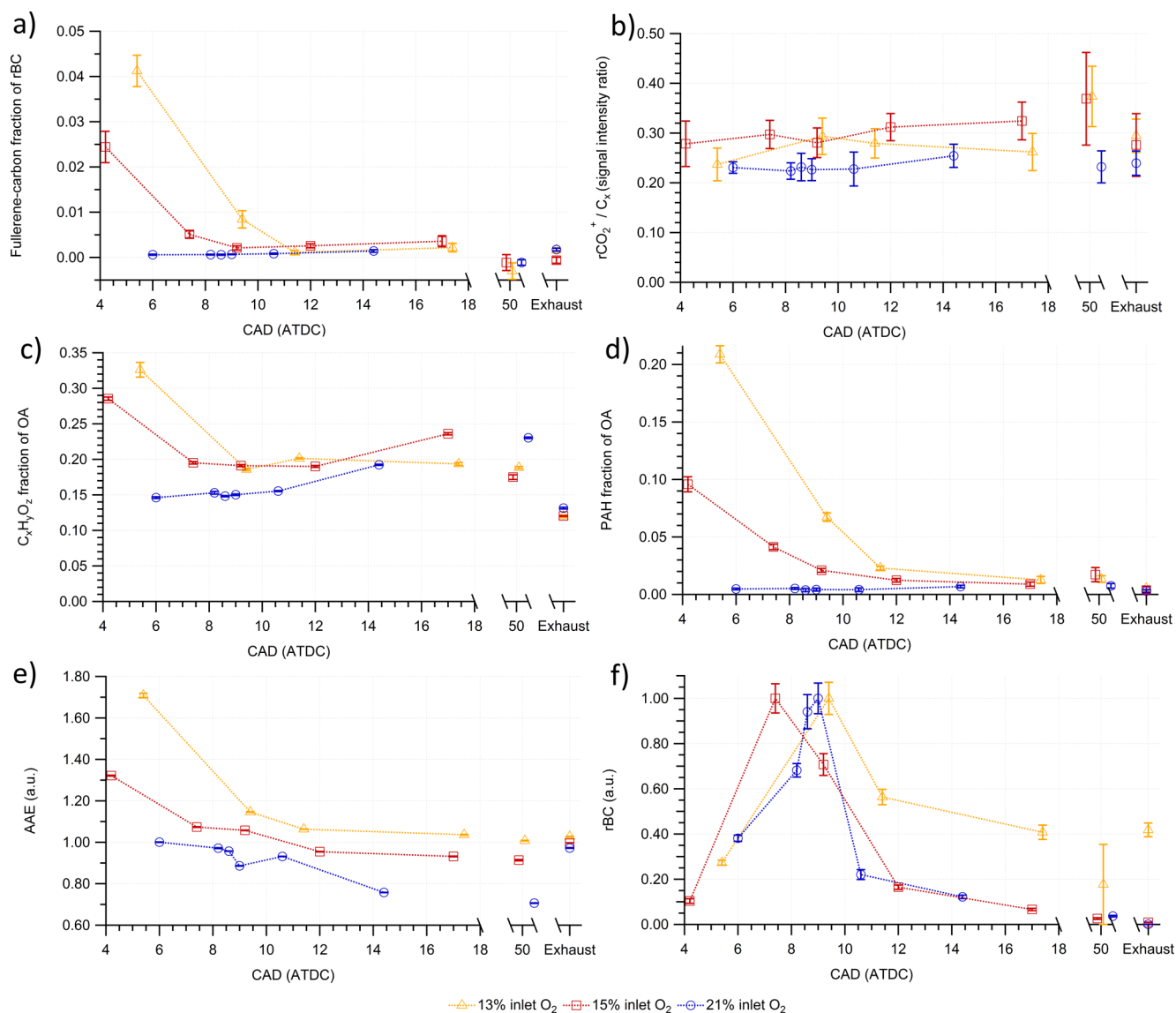


Figure 4. Evolution of soot properties during the combustion cycle and at 21%, 15%, and 13% inlet O_2 concentrations. (a) Fullerene-carbon fraction of rBC. (b) rCO_2^+ normalized to the total refractory C_x^+ (i.e., carbon cluster, signal intensity). (c) Oxidized organic ($C_xH_yO_z^+$) fraction of total OA concentration. (d) PAH fraction of total OA concentration. (e) Variations in AAE with the combustion cycle. (f) rBC normalized to their respective peak in-cylinder concentration. Error bars represent standard errors of the mean.

It was recently shown¹³ that partial premixing of oxygen in benzene (and ethylene) flames introduced high curvature, C_5 -containing fullerenic nanostructures in the soot formed. The C_5 production was suggested to proceed through partial benzene oxidation yielding the phenoxy radical followed by CO loss to produce C_5 . EGR, when used in diesel engines as in this study, allows a higher degree of premixing of O_2 in the soot formation zone similar to the model flame systems discussed above. Thus, we hypothesize that the fullerene-carbon signals correlate with high curvature, C_5 -containing fullerenic-soot nanostructures.⁴⁶ EGR has also been shown to affect exhaust soot properties resulting in a more reactive soot with a higher disorder of the soot nanostructure,⁴⁷ consistent with fullerene-carbon signals in the mass spectra of exhaust soot only being present during combustion with EGR. In previous SP-AMS studies of diesel exhaust, fullerene-carbon signals were commonly not observed.^{45,48} The evolution of soot nanostructures during the diesel combustion cycle has previously been investigated using HR-TEM²³ where it was found that the soot rapidly became

more graphitic as the combustion proceeded, and that after 50 CAD, the gradual increase in graphitic structure was small. Following the discussion of Onasch et al.,⁴⁵ we interpreted the decay in fullerene-carbon signal at 15% and 13% inlet O_2 concentrations to be due to a gradual ordering of the soot nanostructure, analogous to the results of Li et al.²³ The low signal from fullerene-carbon clusters in the late combustion cycle and exhaust is consistent with graphitic soot and reduced content of fullerenic nanostructures.

The importance of the soot nanostructure for reactivity and oxidation rates has been well documented.^{10,49} Shorter graphene layer planes increase the reactive carbon layer edge sites and fullerenic nanostructures have weaker C–C bonds due to the curvature of the molecules which increases the accessibility for oxidation by O_2 and OH.⁴⁹ We therefore hypothesize that the soot associated with the fullerene-carbon signals in the SP-AMS was oxidized (removed) more rapidly than soot that did not produce a fullerene-carbon signal. This

could explain the lower fullerene-carbon signals from soot extracted late in the combustion cycle and in the exhaust.

In addition to rBC, the refractory part of the mass spectrum included considerable signal intensity from CO_2^+ ions. The refractory CO_2^+ (rCO_2^+) intensity to that of the refractory C_x^+ signal intensity varied only weakly over the combustion cycle (Figure 4b), with slightly higher ratios when EGR was applied to the engine. We also observed refractory C_3O_2^+ ions. The signal from rC_3O_2^+ ions was approximately ten times lower than the ion signal from rCO_2^+ . However, and more importantly, the rC_3O_2^+ and rCO_2^+ signals showed trends in the combustion cycle that were similar to those of X-ray photoelectron spectroscopy analyses of oxygenated surface functional groups reported in the literature.²⁴ We hypothesize that these refractory oxygen-containing ion fragments observed in the SP-AMS mass spectra arose as a result of the partial oxidation of soot cores, and that the ions originated from oxygenated functional groups in the soot core carbon nanostructure and on the soot core surface as suggested previously in laboratory⁵⁰ as well as ambient⁵¹ measurements.

When EGR was applied, the fraction of nonrefractory oxidized organic fragments ($\text{C}_x\text{H}_y\text{O}_z^+$) to the total OA decayed from an initially high fraction ($\sim 30\%$) down to $\sim 15\%$ as the combustion proceeded (Figure 4c). This may have been a result of the higher availability of O_2 during the early combustion cycle due to the increased premixing with EGR. However, because this decay was correlated with the decay in the fullerene-carbon signal, it could be associated with decreased reactivity of the soot surfaces as the combustion proceeded. With no EGR, the initial contribution from oxidized organics to the total OA was low and instead, a gradual increase was observed as the combustion proceeded. This resulted in a small increase of the oxidized organic fraction of OA in the exhaust at 21% inlet O_2 concentration relative to 15% and 13% inlet O_2 concentrations. These observations indicate that the mechanism responsible for the higher fraction of nonrefractory oxidized organics in the exhaust at 21% inlet O_2 concentration compared to the EGR cases could be the higher availability of O_2 during the late cycle. A small fraction of the signal originating from surface oxides as described above for rCO_x^+ may have been volatile enough to be vaporized at 600 °C. This would explain the part of the signal in the nonrefractory spectra that varied only weakly with CAD.

Figure 4d shows the quantified mass fraction of all selected PAHs to the total OA mass. With no EGR, PAHs made up only a small fraction of the total in-cylinder OA. With EGR, PAHs made up a considerable fraction of OA in the soot formation dominated phase. The PAH fraction of OA was 18.1% at 13% inlet O_2 concentration and 8.9% at 15% inlet O_2 concentration in the soot formation phase. In the soot oxidation phase and exhaust, the PAH fraction of OA was low at all three EGR levels but increased with EGR.

The in-cylinder PAH fraction of OA was strongly correlated with the fullerene-carbon signal fraction of rBC ($r = 0.91$) which suggests that these form from similar in-cylinder combustion processes. Soot formation is linked to the formation of moderately sized PAHs.⁹ Considering only the growth of PAHs and soot particles, we propose that the low concentration of PAHs (MW 202-300) at 21% inlet O_2 concentration in the soot formation phase was a result of faster particle inception and surface reactions rates (i.e., a much more rapid soot formation) than PAH formation rates. On the other hand, we propose that at 15% and 13% inlet O_2

concentrations, the elevated PAH concentrations were the direct result of lower combustion temperatures, which allowed the PAH concentration to accumulate due to slower particle inception and reactions with soot surfaces. A previous in-cylinder PAH diagnostics study using laser-induced fluorescence showed that the PAH residence time in the flame-jet before the onset of soot formation increased drastically with increasing EGR, from tens of microseconds with no EGR to milliseconds with high EGR (12.7% O_2).¹⁶ Extending the argumentation to include soot properties, when introducing EGR, longer residence times of PAHs and soot precursors coupled with lower flame temperatures would also be important for the formation of fullerene nanostructures.

Finally, we observed variations in the optical properties of the in-cylinder soot (Figure 4e) by analyzing the absorption angstrom exponent (AAE), a measure of the absorption wavelength dependency of the particles. The AAE was highest in the early stages of combustion and progressively became smaller as the combustion proceeded. Remarkable transitions in AAE were observed when reducing the inlet O_2 concentration. In the soot formation dominated phase, the AAE was 1.7 at 13% inlet O_2 concentration, 1.3 at 15% inlet O_2 concentration, and 1.0 at 21% inlet O_2 concentration. In the soot oxidation dominated phase, AAE was 1.1, 1.0, and close to 0.8 at 13%, 15%, and 21% inlet O_2 concentrations, respectively. The order was similar in the exhaust but the differences were smaller. At 21% inlet O_2 concentration in the late combustion cycle, the particle concentrations were very low and the AAE measurement was most likely affected by the background particles (see SI) that were released from the sampling valve without combustion in the motored mode. These background particles had a larger size in the SMPS and appeared to be associated with a lower AAE than the particles in the exhaust.

We conclude that the low AAE found in the diesel exhaust soot was due to a gradual decrease in AAE as the combustion proceeded. These variations in AAE resemble the trends associated with increasing graphitization of the soot. Correlating the observed in-cylinder soot AAE with SP-AMS data, we concluded that the overall OA to BC ratio of the in-cylinder diesel soot showed a low correlation ($r = 0.08$) with the observed changes in AAE (OA originates mostly from lubrication oil). However, when grouped into their respective OA families, the fraction of OA belonging to aliphatic-like fragments ($\text{C}_x\text{H}_{y>x}^+$) was inversely correlated ($r = -0.82$) with AAE, while the fraction of PAHs ($r = 0.93$), aromatic-like ($\text{C}_x\text{H}_{y\leq x}^+$) fragments ($r = 0.84$), and oxidized organic ($\text{C}_x\text{H}_y\text{O}_z^+$) fragments ($r = 0.68$) were positively correlated with AAE. In addition to nonrefractory components, a strong correlation between AAE and the fullerene-carbon fraction ($r = 0.91$) and midcarbon fraction of rBC ($r = 0.90$) was observed.

It has previously been shown that variations in AAE can be related to nanostructural differences, with reported values of $\text{AAE} \approx 2$ for fullerene soot⁵² and $\text{AAE} \approx 2$ for spark discharge soot with high curvature nanostructure.⁵³ Fullerene-carbons were exclusively observed during IR laser vaporization with the SP-AMS. The correlation between fullerene-carbons and AAE also suggests that the intrinsic properties of the soot core could have caused the variations in AAE, in addition to variations caused by UV-absorbing organics such as PAHs.

Implications. Evidence of fullerene soot signatures in SP-AMS mass spectra from ambient air have been recently reported.⁵⁴ This stresses the importance of understanding the mechanisms behind the formation of fullerene soot and

associated organics such as PAHs. In addition, it merits further studies on the removal efficiency and transformation of fullerene soot in DPFS, as well as on the toxicological responses, atmospheric transformation and climate relevance of such emissions.

Previous studies with EGR have highlighted an increased reactivity toward oxidation in exhaust soot.^{55,56} The presence of fullerene-carbon clusters in our SP-AMS mass spectra implies that EGR leads to the formation of high tortuosity (high curvature) soot nanostructures. To elucidate the formation mechanisms of fullerene soot in diesel engines, studies on soot formation using well-defined premixed flames¹³ and shock tubes⁵⁷ may thus prove highly relevant. We found that the fullerene signals were reduced as combustion proceeded. Future studies should evaluate if this is due to preferential removal by oxidation of these structures or to a gradual conversion toward more graphitized soot nanostructures.

The results have important implications for emission control systems in modern vehicles. The oxidation reactivity of soot is a key input parameter when designing DPFS which can effectively reduce BC emissions.⁵⁸ It is well-known that the soot nanostructure affects the oxidation reactivity.^{10,56} Diesel oxidation catalysts will reduce the PAH concentration. However, DPFS can increase the emissions of some nitro-PAHs.^{59,60} The influence of EGR on soot nanostructure and concentration of PAHs merits further studies on how exhaust after-treatment can impact the final emitted aerosol properties. We also found altered optical properties of diesel soot with high fullerene-carbon signals. If these can be definitively linked to fullerene nanostructures, it will affect the direct radiative forcing and the accuracy of BC source apportionment based on AAE for such emissions.

The blending of increasing fractions of oxygen containing FAME (fatty acid methyl esters) biodiesel into fossil diesel is currently encouraged to mitigate CO₂ emissions. FAME is associated with reduced particle emissions compared to fossil diesel⁶¹ but was recently found to be associated with increased fractions of high tortuosity nanostructures¹² and increased in vitro toxicity.⁶² The formation of high tortuosity fullerene soot nanostructures has been linked to the premixing of fuel and oxygen in the soot formation zone.¹³ EGR results in increased premixing of fuel and air, while biodiesel provides oxygen from the fuel. If diesel soot reactivity increases with EGR and biodiesel content, it may be possible to increase the efficiency of soot removal in DPFS.

We propose that future research should include in-cylinder sampling with the FSV and sampling at different stages in the exhaust aftertreatment system, combined with the SP-AMS and the mass-spectrometric signatures developed here. Such studies would involve novel engine concepts (e.g., low temperature combustion) and biodiesel fuels, and would have the potential to provide novel information on in-cylinder chemistry. This information can aid in the design of combustion systems, which ultimately influences emissions, climate effects and particle toxicity. In addition, adding online tandem mobility-mass measurements⁶³ downstream the FSV would allow simultaneous measurements of the evolution of particle composition and morphology over the combustion cycle.

■ ASSOCIATED CONTENT

■ Supporting Information

The Supporting Information is available free of charge on the ACS Publications website at DOI: 10.1021/acs.est.6b03391.

NO_x vs CAD; Dilution system and experimental setup; The fast gas-sampling valve (FSV); SP-AMS setup, calibration and data analysis; SMPS mass weighted size distributions in late cycle and exhaust; rC_x⁺ and BC correlation; Adjusting for gas phase CO₂ and CHO; Origin of the organic aerosol: lube oil vs diesel; Refractory fullerene-carbon signal vs nonrefractory background signal (PDF)

■ AUTHOR INFORMATION

Corresponding Author

*Phone: +46 462220892; fax: +46 462224431; e-mail: vilhelm.malmberg@design.lth.se.

Notes

The authors declare no competing financial interest.

■ ACKNOWLEDGMENTS

This research was financed by Metalund, the FORTE Centre for Medicine and Technology for Working Life and Society, GenDies at the Competence Center for the Combustion Processes, Lund University and the Swedish Energy Agency (Project number 10738150289), and The Swedish Research Council VR project nr. 2013-5021. We acknowledge Volvo AB for providing the FSV hardware, Scania CV AB for providing the engine and Jan Eismark (Volvo AB), Timothy Benham (Chalmers University of Technology) and Mats Bengtsson (Lund University) for their technical support, Tim Onasch for discussions on the SP-AMS data, and Bengt Johansson for his contribution to the experimental procedure.

■ REFERENCES

- (1) Salvi, S.; Blomberg, A.; Rudell, B.; Kelly, F.; Sandstrom, T.; Holgate, S. T.; Frew, A. Acute inflammatory responses in the airways and peripheral blood after short-term exposure to diesel exhaust in healthy human volunteers. *Am. J. Respir. Crit. Care Med.* **1999**, *159* (3), 702–709.
- (2) Riedl, M.; Diaz-Sanchez, D. Biology of diesel exhaust effects on respiratory function. *J. Allergy Clin. Immunol.* **2005**, *115* (2), 221–228.
- (3) Cancer, I. A. f. R. o., IARC: Diesel engine exhaust carcinogenic. *Press release* **2012**, (213).
- (4) IPCC. *Climate Change 2013: The Physical Science Basis. Contribution of Working Group I to the Fifth Assessment Report of the Intergovernmental Panel on Climate Change*; Cambridge University Press: Cambridge, 2013; p 1535.
- (5) Mitchell, D. L.; Pinson, J. A.; Litzinger, T. A. The effects of simulated EGR via intake air dilution on combustion in an optically accessible DI diesel engine. *SAE Tech. Pap. Ser.* **1993**, 932798.
- (6) Aronsson, U.; Chartier, C.; Andersson, Ö.; Johansson, B.; Sjöholm, J.; Wellander, R.; Richter, M.; Alden, M.; Miles, P. C. Analysis of EGR effects on the soot distribution in a heavy duty diesel engine using time-resolved laser induced incandescence. *SAE Int. J. Engines* **2010**, *3* (2), 137–155.
- (7) Akihama, K.; Takatori, Y.; Inagaki, K.; Sasaki, S.; Dean, A. M. Mechanism of the smokeless rich diesel combustion by reducing temperature. *SAE Tech. Pap. Ser.* **2001**, 2001–01–0655.
- (8) Tree, D. R.; Svensson, K. I. Soot processes in compression ignition engines. *Prog. Energy Combust. Sci.* **2007**, *33* (3), 272–309.
- (9) Wang, H. Formation of nascent soot and other condensed-phase materials in flames. *Proc. Combust. Inst.* **2011**, *33* (1), 41–67.
- (10) Yehliu, K.; Vander Wal, R. L.; Armas, O.; Boehman, A. L. Impact of fuel formulation on the nanostructure and reactivity of diesel soot. *Combust. Flame* **2012**, *159* (12), 3597–3606.
- (11) Song, J.; Alam, M.; Boehman, A. L. Impact of alternative fuels on soot properties and DPF regeneration. *Combust. Sci. Technol.* **2007**, *179* (9), 1991–2037.

- (12) Savic, N.; Rahman, M.; Miljevic, B.; Saathoff, H.; Naumann, K.; Leisner, T.; Riches, J.; Gupta, B.; Motta, N.; Ristovski, Z. Influence of biodiesel fuel composition on the morphology and microstructure of particles emitted from diesel engines. *Carbon* **2016**, *104*, 179–189.
- (13) Huang, C.-H.; Vander Wal, R. L. Partial premixing effects upon soot nanostructure. *Combust. Flame* **2016**, *168*, 403–408.
- (14) Ristovski, Z. D.; Miljevic, B.; Surawski, N. C.; Morawska, L.; Fong, K. M.; Goh, F.; Yang, I. A. Respiratory health effects of diesel particulate matter. *Respirology* **2012**, *17* (2), 201–212.
- (15) Bowditch, F. W. A new tool for combustion research a quartz piston engine. *SAE Technical Paper* **1961**, 610002.
- (16) Bobba, M. K.; Musculus, M. P. B. Laser diagnostics of soot precursors in a heavy-duty diesel engine at low-temperature combustion conditions. *Combust. Flame* **2012**, *159* (2), 832–843.
- (17) Leermakers, C. A. J.; Musculus, M. P. B. In-cylinder soot precursor growth in a low-temperature combustion diesel engine: Laser-induced fluorescence of polycyclic aromatic hydrocarbons. *Proc. Combust. Inst.* **2015**, *35* (3), 3079–3086.
- (18) Dec, J. E. Soot distribution in a DI diesel engine using 2-D imaging of laser-induced incandescence, elastic scattering, and flame luminosity. *SAE Tech. Pap. Ser.* **1992**, 920115.
- (19) Dec, J. E.; Kelly-Zion, P. L. The effects of injection timing and diluent addition on late-combustion soot burnout in a DI diesel engine based on simultaneous 2-D imaging of OH and soot. *SAE Tech. Pap. Ser.* **2000**, 2000–01–0238.
- (20) Zhao, H.; Ladommatos, N. Optical diagnostics for soot and temperature measurement in diesel engines. *Prog. Energy Combust. Sci.* **1998**, *24* (3), 221–255.
- (21) Zhang, R.; Kook, S. Influence of fuel injection timing and pressure on in-flame soot particles in an automotive-size diesel engine. *Environ. Sci. Technol.* **2014**, *48* (14), 8243–50.
- (22) Piphoo, M. J.; Ambs, J. L.; Kittelson, D. In-cylinder measurements of particulate formation in an indirect injection diesel engine. *SAE Tech. Pap. Ser.* **1986**, 860024.
- (23) Li, Z.; Song, C.; Song, J.; Lv, G.; Dong, S.; Zhao, Z. Evolution of the nanostructure, fractal dimension and size of in-cylinder soot during diesel combustion process. *Combust. Flame* **2011**, *158* (8), 1624–1630.
- (24) Wang, L.; Song, C.; Song, J.; Lv, G.; Pang, H.; Zhang, W. Aliphatic C–H and oxygenated surface functional groups of diesel in-cylinder soot: Characterizations and impact on soot oxidation behavior. *Proc. Combust. Inst.* **2013**, *34* (2), 3099–3106.
- (25) Zhang, R.; Khalizov, A. F.; Pagels, J.; Zhang, D.; Xue, H.; McMurry, P. H. Variability in morphology, hygroscopicity, and optical properties of soot aerosols during atmospheric processing. *Proc. Natl. Acad. Sci. U. S. A.* **2008**, *105* (30), 10291–10296.
- (26) Peng, J.; Hu, M.; Guo, S.; Du, Z.; Zheng, J.; Shang, D.; Zamora, M. L.; Zeng, L.; Shao, M.; Wu, Y.-S. Markedly enhanced absorption and direct radiative forcing of black carbon under polluted urban environments. *Proc. Natl. Acad. Sci. U. S. A.* **2016**, *113* (16), 4266–4271.
- (27) Bertoli, C.; Del Giacomo, N.; Beatrice, C. Evaluation of combustion behavior and pollutants emission of advanced fuel formulations by single cylinder engine experiments. *SAE Tech. Pap. Ser.* **1998**, 982492.
- (28) Karagiorgis, S.; Collings, N.; Glover, K.; Coghlan, N.; Petridis, A. Residual gas fraction measurement and estimation on a homogeneous charge compression ignition engine utilizing the negative valve overlap strategy. *SAE Tech. Pap. Ser.* **2006**, 2006–01–3276.
- (29) Shen, M.; Malmberg, V.; Gallo, Y.; Waldheim, B. B. O.; Nilsson, P.; Eriksson, A.; Pagels, J.; Andersson, O.; Johansson, B. Analysis of soot particles in the cylinder of a heavy duty diesel engine with high EGR. *SAE Tech. Pap. Ser.* **2015**, 2015–24–2448.
- (30) Onasch, T. B.; Trimborn, A.; Fortner, E. C.; Jayne, J. T.; Kok, G. L.; Williams, L. R.; Davidovits, P.; Worsnop, D. R. Soot particle aerosol mass spectrometer: development, validation, and initial application. *Aerosol Sci. Technol.* **2012**, *46* (7), 804–817.
- (31) DeCarlo, P. F.; Kimmel, J. R.; Trimborn, A.; Northway, M. J.; Jayne, J. T.; Aiken, A. C.; Gonin, M.; Fuhrer, K.; Horvath, T.; Docherty, K. S. Field-deployable, high-resolution, time-of-flight aerosol mass spectrometer. *Anal. Chem.* **2006**, *78* (24), 8281–8289.
- (32) Wang, X.; Song, C.; Lv, G.; Song, J.; Li, H.; Li, B. Evolution of in-cylinder polycyclic aromatic hydrocarbons in a diesel engine fueled with n-heptane and n-heptane/toluene. *Fuel* **2015**, *158*, 322–329.
- (33) Gallo, Y.; Simonsson, J.; Lind, T.; Bengtsson, P.-E.; Bladh, H.; Andersson, O. A study of in-cylinder soot oxidation by laser extinction measurements during an EGR-sweep in an optical diesel engine. *SAE Tech. Pap. Ser.* **2015**, 2015–01–0800.
- (34) Liu, P. S.; Deng, R.; Smith, K. A.; Williams, L. R.; Jayne, J. T.; Canagaratna, M. R.; Moore, K.; Onasch, T. B.; Worsnop, D. R.; Deshler, T. Transmission efficiency of an aerodynamic focusing lens system: Comparison of model calculations and laboratory measurements for the Aerodyne Aerosol Mass Spectrometer. *Aerosol Sci. Technol.* **2007**, *41* (8), 721–733.
- (35) Jayne, J. T.; Leard, D. C.; Zhang, X.; Davidovits, P.; Smith, K. A.; Kolb, C. E.; Worsnop, D. R. Development of an aerosol mass spectrometer for size and composition analysis of submicron particles. *Aerosol Sci. Technol.* **2000**, *33* (1–2), 49–70.
- (36) Drinovec, L.; Močnik, G.; Zotter, P.; Prévôt, A.; Ruckstuhl, C.; Coz, E.; Rupakheti, M.; Sciare, J.; Müller, T.; Wiedensohler, A. The “dual-spot” Aethalometer: An improved measurement of aerosol black carbon with real-time loading compensation. *Atmos. Meas. Tech.* **2015**, *8* (5), 1965–1979.
- (37) Willis, M. D.; Lee, A. K. Y.; Onasch, T. B.; Fortner, E. C.; Williams, L. R.; Lambe, A. T.; Worsnop, D. R.; Abbatt, J. P. D. Collection efficiency of the Soot-Particle Aerosol Mass Spectrometer (SP-AMS) for internally mixed particulate black carbon. *Atmos. Meas. Tech.* **2014**, *7* (5), 4507–4516.
- (38) Herring, C. L.; Faiola, C. L.; Massoli, P.; Sueper, D.; Erickson, M. H.; McDonald, J. D.; Simpson, C. D.; Yost, M. G.; Jobson, B. T.; VanReken, T. M. New methodology for quantifying polycyclic aromatic hydrocarbons (PAHs) using high-resolution aerosol mass spectrometry. *Aerosol Sci. Technol.* **2015**, *49* (11), 1131–1148.
- (39) Huestis, E.; Erickson, P. A.; Musculus, M. P. In-cylinder and exhaust soot in low-temperature combustion using a wide-range of EGR in a heavy-duty diesel engine. *SAE Tech. Pap. Ser.* **2007**, 2007–01–4017.
- (40) Gallo, Y.; Malmberg, V. B.; Simonsson, J.; Svensson, E.; Shen, M.; Bengtsson, P.-E.; Pagels, J.; Tunér, M.; Garcia, A.; Andersson, Ö. Investigation of late-cycle soot oxidation using laser extinction and in-cylinder gas sampling at varying inlet oxygen concentrations in diesel engines. *Fuel* Accepted for publication, 7 December **2016**, 19330810.1016/j.fuel.2016.12.013.
- (41) Canagaratna, M. R.; Jayne, J. T.; Ghertner, D. A.; Herndon, S.; Shi, Q.; Jimenez, J. L.; Silva, P. J.; Williams, P.; Lanni, T.; Drewnick, F. Chase studies of particulate emissions from in-use New York City vehicles. *Aerosol Sci. Technol.* **2004**, *38* (6), 555–573.
- (42) Tobias, H. J.; Beving, D. E.; Ziemann, P. J.; Sakurai, H.; Zuk, M.; McMurry, P. H.; Zarling, D.; Waytulonis, R.; Kittelson, D. B. Chemical analysis of diesel engine nanoparticles using a nano-DMA/thermal desorption particle beam mass spectrometer. *Environ. Sci. Technol.* **2001**, *35* (11), 2233–2243.
- (43) Massoli, P.; Fortner, E. C.; Canagaratna, M. R.; Williams, L. R.; Zhang, Q.; Sun, Y.; Schwab, J. J.; Trimborn, A.; Onasch, T. B.; Demerjian, K. L. Pollution gradients and chemical characterization of particulate matter from vehicular traffic near major roadways: Results from the 2009 Queens College Air Quality Study in NYC. *Aerosol Sci. Technol.* **2012**, *46* (11), 1201–1218.
- (44) Sakurai, H.; Tobias, H. J.; Park, K.; Zarling, D.; Docherty, K. S.; Kittelson, D. B.; McMurry, P. H.; Ziemann, P. J. On-line measurements of diesel nanoparticle composition and volatility. *Atmos. Environ.* **2003**, *37* (9), 1199–1210.
- (45) Onasch, T. B.; Fortner, E. C.; Trimborn, A. M.; Lambe, A. T.; Tiwari, A. J.; Marr, L. C.; Corbin, J. C.; Mensah, A. A.; Williams, L. R.; Davidovits, P.; Worsnop, D. R. Investigations of SP-AMS carbon ion

distributions as a function of refractory black carbon particle type. *Aerosol Sci. Technol.* **2015**, *49* (6), 409–422.

(46) Goel, A.; Hebggen, P.; Vander Sande, J. B.; Howard, J. B. Combustion synthesis of fullerenes and fullerene nanostructures. *Carbon* **2002**, *40* (2), 177–182.

(47) Xu, Z.; Li, X.; Guan, C.; Huang, Z. Effects of injection timing on exhaust particle size and nanostructure on a diesel engine at different loads. *J. Aerosol Sci.* **2014**, *76*, 28–38.

(48) Dallmann, T.; Onasch, T.; Kirchstetter, T.; Worton, D.; Fortner, E.; Herndon, S.; Wood, E.; Franklin, J.; Worsnop, D.; Goldstein, A. Characterization of particulate matter emissions from on-road gasoline and diesel vehicles using a soot particle aerosol mass spectrometer. *Atmos. Chem. Phys.* **2014**, *14* (14), 7585–7599.

(49) Vander Wal, R. L.; Tomasek, A. J. Soot oxidation: Dependence upon initial nanostructure. *Combust. Flame* **2003**, *134* (1), 1–9.

(50) Corbin, J. C.; Sierau, B.; Gysel, M.; Laborde, M.; Keller, A.; Kim, J.; Petzold, A.; Onasch, T. B.; Lohmann, U.; Mensah, A. A. Mass spectrometry of refractory black carbon particles from six sources: Carbon-cluster and oxygenated ions. *Atmos. Chem. Phys.* **2014**, *14* (5), 2591–2603.

(51) Massoli, P.; Onasch, T. B.; Cappa, C. D.; Nuamaan, I.; Hakala, J.; Hayden, K.; Li, S. M.; Sueper, D. T.; Bates, T. S.; Quinn, P. K. Characterization of black carbon-containing particles from soot particle aerosol mass spectrometer measurements on the R/V Atlantis during CalNex 2010. *J. Geophys. Res. Atmos.* **2015**, *120* (6), 2575–2593.

(52) McMeeking, G.; Fortner, E.; Onasch, T.; Taylor, J.; Flynn, M.; Coe, H.; Kreidenweis, S. Impacts of nonrefractory material on light absorption by aerosols emitted from biomass burning. *J. Geophys. Res. Atmos.* **2014**, *119* (21), 12,272–12,286.

(53) Schnaiter, M.; Horvath, H.; Möhler, O.; Naumann, K. H.; Saathoff, H.; Schöck, O. W. UV-VIS-NIR spectral optical properties of soot and soot-containing aerosols. *J. Aerosol Sci.* **2003**, *34* (10), 1421–1444.

(54) Wang, J.; Onasch, T. B.; Ge, X.; Collier, S.; Zhang, Q.; Sun, Y.; Yu, H.; Chen, M.; Prévôt, A. S.; Worsnop, D. R. Observation of fullerene soot in eastern China. *Environ. Sci. Technol. Lett.* **2016**, *3* (4), 121–126.

(55) Li, X.; Xu, Z.; Guan, C.; Huang, Z. Oxidative reactivity of particles emitted from a diesel engine operating at light load with EGR. *Aerosol Sci. Technol.* **2015**, *49* (1), 1–10.

(56) Al-Qurashi, K.; Boehman, A. L. Impact of exhaust gas recirculation (EGR) on the oxidative reactivity of diesel engine soot. *Combust. Flame* **2008**, *155* (4), 675–695.

(57) Qiu, C.; Khalizov, A. F.; Hogan, B.; Petersen, E. L.; Zhang, R. High sensitivity of diesel soot morphological and optical properties to combustion temperature in a shock tube. *Environ. Sci. Technol.* **2014**, *48* (11), 6444–6452.

(58) Liu, Z. G.; Berg, D. R.; Swor, T. A.; Schauer, J. J. Comparative analysis on the effects of diesel particulate filter and selective catalytic reduction systems on a wide spectrum of chemical species emissions. *Environ. Sci. Technol.* **2008**, *42* (16), 6080–6085.

(59) Liu, Z. G.; Wall, J. C.; Ottinger, N. A.; McGuffin, D. Mitigation of PAH and nitro-PAH emissions from nonroad diesel engines. *Environ. Sci. Technol.* **2015**, *49* (6), 3662–3671.

(60) Heeb, N. V.; Schmid, P.; Kohler, M.; Gujer, E.; Zennegg, M.; Wenger, D.; Wichser, A.; Ulrich, A.; Gfeller, U.; Honegger, P. Secondary effects of catalytic diesel particulate filters: Conversion of PAHs versus formation of nitro-PAHs. *Environ. Sci. Technol.* **2008**, *42* (10), 3773–3779.

(61) Lapuerta, M.; Armas, O.; Rodriguez-Fernandez, J. Effect of biodiesel fuels on diesel engine emissions. *Prog. Energy Combust. Sci.* **2008**, *34* (2), 198–223.

(62) Hedayat, F.; Stevanovic, S.; Milic, A.; Miljevic, B.; Nabi, M. N.; Zare, A.; Bottle, S.; Brown, R. J.; Ristovski, Z. D. Influence of oxygen content of the certain types of biodiesels on particulate oxidative potential. *Sci. Total Environ.* **2016**, *545*, 381–388.

(63) Pagels, J.; Khalizov, A. F.; McMurry, P. H.; Zhang, R. Y. Processing of soot by controlled sulphuric acid and water

condensation—Mass and mobility relationship. *Aerosol Sci. Technol.* **2009**, *43* (7), 629–640.